



3 4456 0331124 4

ORNL/TM-11758



OAK RIDGE
NATIONAL
LABORATORY

MARTIN MARIETTA

Inversion of Chordal Data From the ATF Torsatron

L. R. Baylor
C. H. Ma
S. Hiroe

OAK RIDGE NATIONAL LABORATORY
CENTRAL RESEARCH LIBRARY
CIRCULATION SECTION
4500 ROOM 121
LIBRARY LOAN COPY
DO NOT TRANSFER TO ANOTHER PERSON
If you wish someone else to see this
report, send its name with report and
the library will arrange a loan.

This report has been reproduced directly from the best available copy.

Available to DOE and DCF contractors from the Office of Scientific and Technical Information, P.O. Box 62, Oak Ridge, TN 37831; prices available from (615) 576-8401, FTS 620-8101

Available to the public from the National Technical Information Service, U.S. Department of Commerce, 5285 Port Royal Rd., Springfield, VA 22161.

This report was prepared as an account of work sponsored by an agency of the United States Government. Neither the United States Government nor any agency thereof, nor any of their employees, makes any warranty, express or implied, or assumes any legal liability or responsibility for the accuracy, completeness, or usefulness of any information, apparatus, product, or process disclosed, or represents that its use would not infringe privately owned rights. Reference herein to any specific commercial product, process, or service by trade name, trademark, manufacturer, or otherwise, does not necessarily constitute or imply its endorsement, recommendation, or favoring by the United States Government or any agency thereof. The views and opinions of authors expressed herein do not necessarily state or reflect those of the United States Government or any agency thereof.

ORNL/TM-11758
Dist. Category UC-426

Fusion Energy Division

**INVERSION OF CHORDAL DATA
FROM THE ATF TORSATRON**

L. R. Baylor

C. H. Ma

S. Hiroe

Date Published: February 1991

Prepared for the
Office of Fusion Energy
Budget Activity No. AT 05

Prepared by the
OAK RIDGE NATIONAL LABORATORY
Oak Ridge, Tennessee 37831
managed by
MARTIN MARIETTA ENERGY SYSTEMS, INC.
for the
U.S. DEPARTMENT OF ENERGY
under contract DE-AC05-84OR21400



3 4456 0331124 4

CONTENTS

ABSTRACT	v
1. INTRODUCTION	1
2. INVERSION METHOD	3
3. ATF FIR MULTICHANNEL INTERFEROMETER	5
4. BOLOMETER ARRAY ON ATF	7
5. INVERSION RESULTS	9
5.1 ELECTRON DENSITY PROFILES	9
5.2 RADIATED POWER DENSITY PROFILES	13
5.3 SENSITIVITY ANALYSIS	14
6. SUMMARY	17
ACKNOWLEDGMENTS	18
REFERENCES	19

ABSTRACT

A method to obtain electron density profiles from chordal interferometric measurements of a tokamak plasma has been extended to the non-axisymmetric stellarator geometry of the Advanced Toroidal Facility (ATF) torsatron. The method requires a known magnetic flux surface geometry expressed in spectral form. The method has been applied to both interferometer density data and bolometer irradiance data from ATF, and results are presented. The resulting inverted density profiles are integrated along a horizontal path and compare favorably with line integral measurements of the density. Sensitivities of the resulting profiles to variations in the flux surface geometry and errors in the measurements are discussed.

1. INTRODUCTION

The Advanced Toroidal Facility (ATF) is an $l = 2$ torsatron having 12 field periods designed for studies of plasma stability and confinement in a current-free toroidal device [1]. Two diagnostics on the ATF device measure chordal integrals of plasma quantities that require an inversion to ascertain the local values of these quantities. The first is a multichannel far-infrared (FIR) interferometer system [2] that has been installed on ATF for the purpose of measuring electron density. The second diagnostic is a 15 channel bolometer array [3] that has been borrowed from the PBX-M experiment at the Princeton Plasma Physics Laboratory to measure the radiated power from the plasma. The inversion of these chordal data to a local electron density profile and a radiated power density profile, respectively, is accomplished by a technique extended from an asymmetric inversion method developed for tokamak plasmas [4]. The method is described in detail in Section 2.

In Section 3, we discuss the FIR interferometer system on ATF. The multichannel bolometer array installed on ATF is discussed in Section 4. The results of applying the inversion process to data from these two diagnostics are examined in Section 5. The sensitivity of the method to the flux surface geometry determined from the plasma beta is investigated, as is the sensitivity of the resulting profiles to uncertainties in the measured data. Examples of resulting electron density profiles obtained from plasmas with different heating and fueling methods are shown. Important density parameters such as profile peakedness, central density, and line-integrated density are calculated from the inverted profiles and presented. An example of the resulting temporal evolution of the radiated power density profile for an ATF discharge is also shown.

2. INVERSION METHOD

Here we review the details of the asymmetric inversion technique developed for tokamaks [4]. The basic principle of the method is to divide the flux surface geometry into shells that are assumed to have a constant particle density or radiated power density. The measured chordal data are interpolated to provide data for chords that pass through the center of each shell at the horizontal midplane. The path length of the interpolated chords through the shells is calculated, and the local density within the shell is determined by starting at the outermost shell and working toward the innermost shell. This is done for the chords on both the inside and outside of the magnetic axis independently, which allows for an asymmetric profile.

The measured chordal signal (assumed here to be the interferometer signal) can be written as

$$\int n_e(r)dl = N_e L$$

where $N_e = n_{e(n,m)}$ is the electron density matrix, $L = l_{n,m}$ is the path length matrix for the flux surface geometry being analyzed, n is the zone index, and m is the subzone index. As described in the original derivation [4], the choice of number of zones (shells) n is flexible and in our case is chosen to be 10, thus leading to the number of chords, $2n$, to be 20. The actual number of measured chords is fewer than 20; therefore, we use a cubic spline fit between the measured values to arrive at an interpolated chordal value at the center of each flux surface zone.

The inversion process starts from the outermost interpolated chord in each zone. The line-integrated densities for each chord can be expressed as

$$\left(\int n_e dl \right)_1 = n_{e(1,1)} l_{1,1}$$

$$\left(\int n_e dl \right)_2 = n_{e(1,2)} l_{1,2} + n_{e(2,1)} l_{2,1}$$

⋮

$$\left(\int n_e dl\right)_{2n-1} = n_{e(1,2n-1)}l_{1,2n-1} + n_{e(2,2n-2)}l_{2,2n-2}$$

$$\left(\int n_e dl\right)_{2n} = n_{e(1,2n)}l_{1,2n}$$

In our calculation, any in/out asymmetry of the electron density (i.e. difference in the calculated densities $n_e(1, 1)$ and $n_e(1, 2n)$ of the first and last equations above) is distributed linearly along the major axis. It would also be possible to distribute the asymmetry with a cosine or other distribution if desired. Once the subzone densities ($n_{e(1,j)}$) in the first zone (outermost shell) are determined, the same operation can be performed on the next zone to determine ($n_{e(2,j)}$) and so on. The method will work on density profiles of any shape, including hollow, and is limited in resolution by the number of chordal measurements and the number of flux surface zones chosen in the plasma.

3. ATF FIR MULTICHANNEL INTERFEROMETER

The multichannel interferometer on ATF is a 15 vertical chord system based on a pair of optically pumped difluoromethane (CH_2F_2) lasers operating at a wavelength of $214\ \mu\text{m}$ [2]. The vertical chords are located in the $\phi = 0$ toroidal plane of ATF, as shown in Fig. 1. The input beam is expanded with reflective optics and transmitted through most of the plasma cross-section. After passing through the plasma, the probing beam is mixed with a reference beam and detected by an array of Schottky diode detectors. The phase shift between the

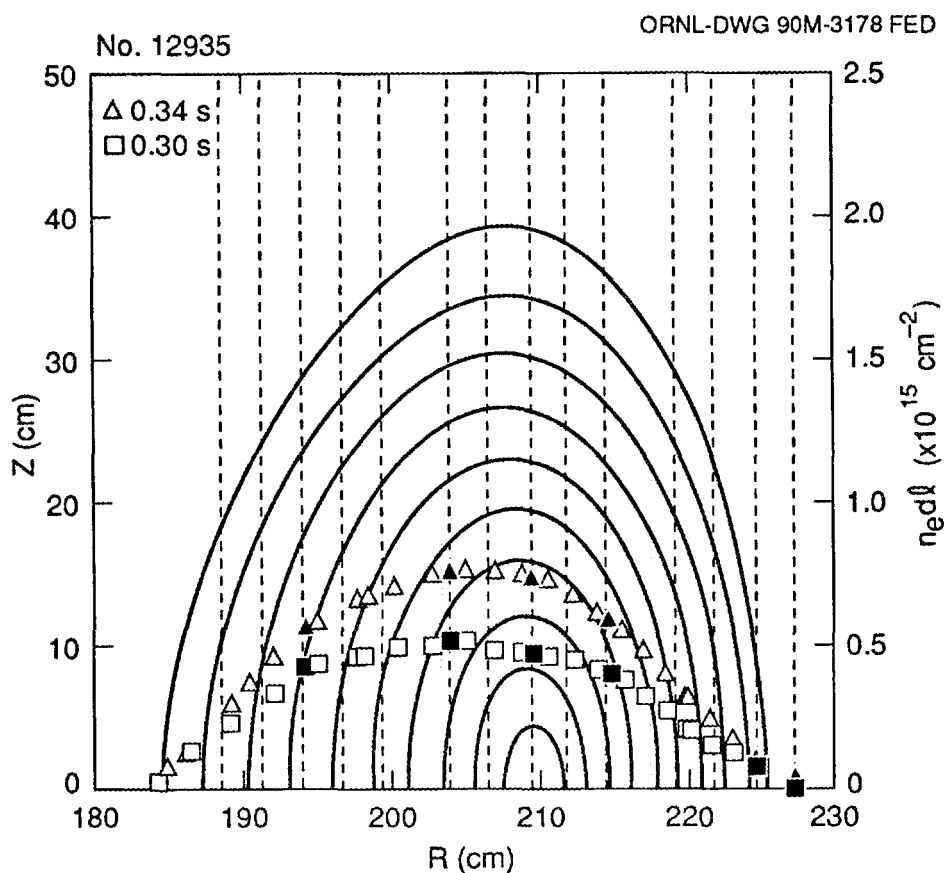


Fig. 1. Flux surface geometry of the ATF device (upper half) with the paths of the multichannel FIR interferometer system shown as dashed vertical lines. The interferometer data (solid points) and spline fit through the data for two times during a discharge with pellet injection are overlaid. The later time is just after a deuterium pellet is injected into the plasma.

output of the signal detectors and the reference signal, which is proportional to the line-integrated electron density, is then measured. The interferometer system has been operated to date with up to seven working detectors, limited by detector availability.

A complete 2π phase shift in the probing beam with respect to the reference beam corresponds to a line integral density of $1.1 \times 10^{15} \text{ cm}^{-2}$. The line-integrated density often exceeds this value and thus leads to a fringe loss in the measured interferometer data. Software is used to recover the lost fringes and has been successful in recovering the data from high-density discharges with line integral densities exceeding $6.0 \times 10^{15} \text{ cm}^{-2}$.

Strong density gradients in the plasma are known to cause a refraction of the probing FIR interferometer beam. This is especially prominent near the plasma edge during neutral beam injection (NBI). Ray tracing calculations of the amount of refraction [5] indicate that shifts of the beam to the outer channels by as much as 2 cm can be realized. This refraction in the beam is not currently taken into account in the density inversion in a self-consistent manner but is left for a future upgrade in the inversion technique.

4. BOLOMETER ARRAY ON ATF

The multichannel bolometer used on ATF is a 15 channel array that views plasma irradiance vertically in the $\phi = 0$ plane. The bolometer is configured such that the detector chordal lines of sight are spread in a fan shape as shown in Fig. 2, which provides a resolution of 4 cm at the horizontal midplane. The bolometer itself has been borrowed from the PBX-M experiment [3] and was installed on ATF to determine the radially resolved radiated power density profile.

Each detector channel of the bolometer measures the irradiance along its line of sight through the plasma. The detectors are resistive elements that change resistance with an accumulated incident heat flux. The instantaneous incident

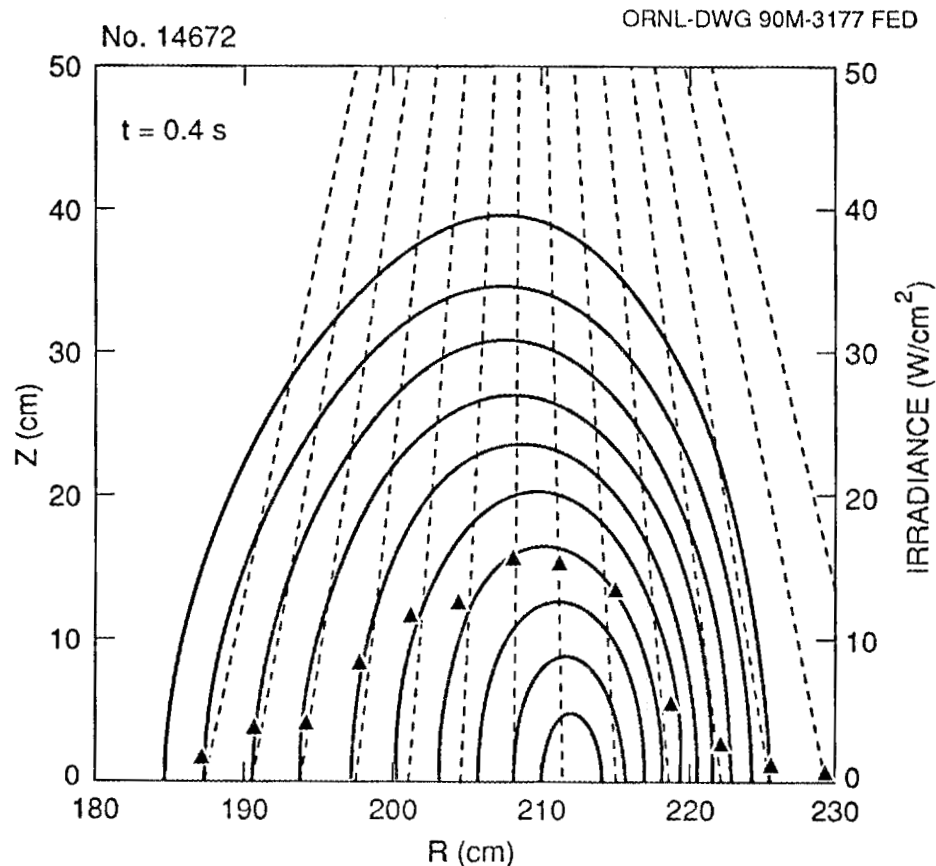


Fig. 2. Flux surface geometry (upper half) and bolometer channel lines of sight on ATF. The values of irradiance for each chord (Δ) are plotted as a function of the position of the chord crossing at the horizontal midplane.

power is obtained by digitally smoothing and differentiating the resistance signal from the detector. Inversion of the irradiance data is required to give a profile of the local radiated power density. Integration of the inverted profile over the plasma volume then gives the total radiated power from the plasma.

Some simplifying assumptions have been made in inverting the bolometer array data from ATF. The bolometer detectors view the plasma in a cone with a width in the toroidal direction of approximately 20 cm, which corresponds to $\phi = \pm 1.5^\circ$. The small change in flux surface geometry over the toroidal viewing extent is ignored in the inversion process (i.e. the plasma viewed by the bolometer is assumed to be axisymmetric). The other primary assumption is that the viewing chord of each bolometer detector is assumed to have a constant rectangular cross-section through the plasma. This ignores the spreading of the viewing area that occurs because of the apertured detector acting like a point source. The R^2 change in differential viewing area (where R is the distance of the detector from the plasma element) is fairly small owing to the distance of the bolometer array from the plasma.

5. INVERSION RESULTS

The inversion method described in Section 2 has been used to generate density profiles and radiated power profiles for a variety of plasma conditions in ATF. The flux surface geometry used to invert the chordal data is determined from the three-dimensional (3-D) equilibrium code VMEC [6] and uses the experimentally determined pressure profiles derived from Thomson scattering [7] measurements when available. The flux surface geometry calculated from VMEC is stored in the spectral form given by

$$R(\rho, \theta, \phi) = \sum_m \sum_n R_{mn}(\rho) \cos(m\theta - n\phi)$$

$$Z(\rho, \theta, \phi) = \sum_m \sum_n Z_{mn}(\rho) \sin(m\theta - n\phi),$$

where ρ is a radial coordinate labeling a flux surface, θ is a poloidal coordinate, and ϕ is a toroidal coordinate. The coefficients of the transformation are then stored for a discrete set of ρ values. The path lengths are calculated using the TRACK subroutines [8], which contain an efficient algorithm for determining intersections of a straight trajectory with a set of nested flux surfaces represented in spectral form.

5.1 ELECTRON DENSITY PROFILES

As described in Section 2, the inversion technique uses a cubic spline fit through the measured data points to generate an interpolated chordal value at the center of each flux surface zone. Figure 1 shows both the measured line integral density and the interpolated data points for two times during an electron-cyclotron-heated (ECH) discharge with pellet injection. One can see from the increase in the central channels that the density profile must be more peaked after the pellet is injected.

The temporal evolution of the density profile has been determined by running a code using the inversion method for a large number of time slices throughout the discharge. An example of the resulting density profile evolution is shown

in Fig. 3 for a discharge that starts out with ECH and follows with 200 ms of NBI [9]. The density rises rapidly during NBI and the profile remains relatively flat until the plasma undergoes a thermal collapse at 0.43s, which leads to a transiently peaked profile.

A useful parameter for plasma confinement studies derived from the inverted density profile is the density profile peaking factor

$$n_{\text{pkd}} = \frac{n_{e0}}{\langle n_e \rangle_{\text{vol}}}$$

where n_{e0} is the electron density at the magnetic axis and $\langle n_e \rangle_{\text{vol}}$ is the volume-averaged electron density. The temporal evolution of the peaking factor, central density, and total number of plasma electrons is shown in Fig. 4 for the ATF discharge with NBI that is shown in Fig. 3.

An example of the density profile evolution from the inversion method for an ECH-only discharge is shown in Fig. 5. In this discharge a 1 mm deuterium

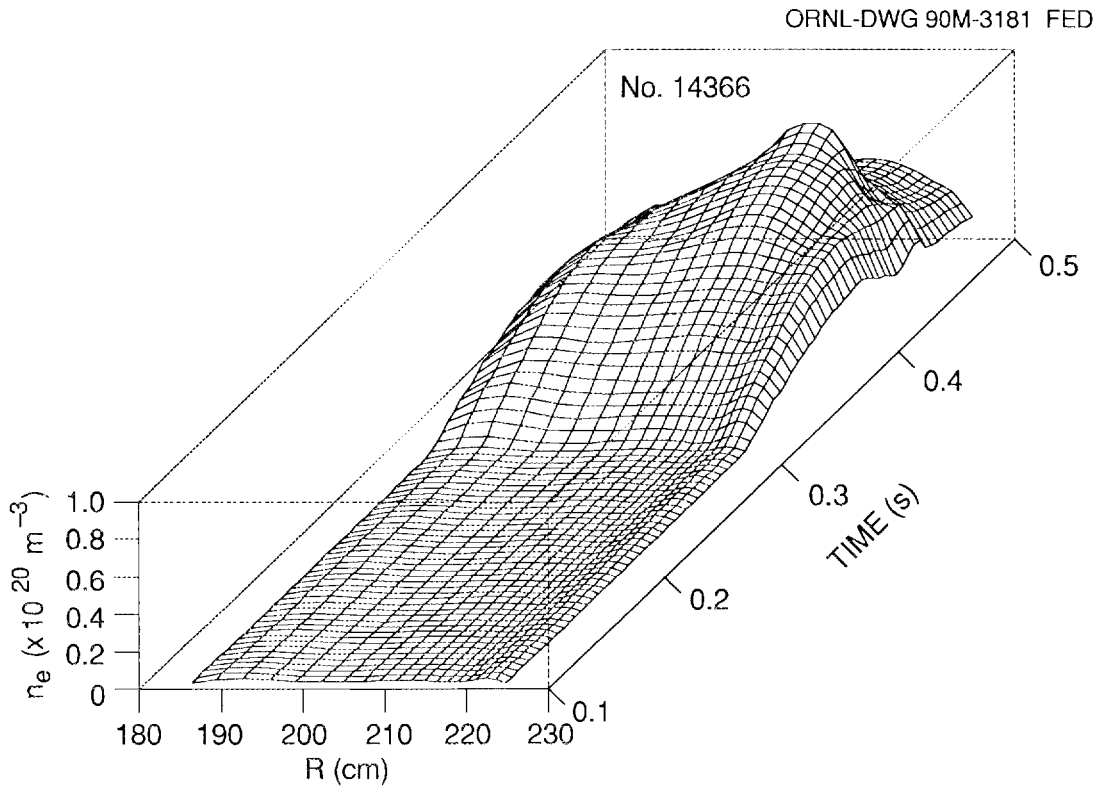


Fig. 3. The density profile evolution calculated from the inversion method for a neutral beam injection discharge. Neutral beam injection begins at 0.3 s.

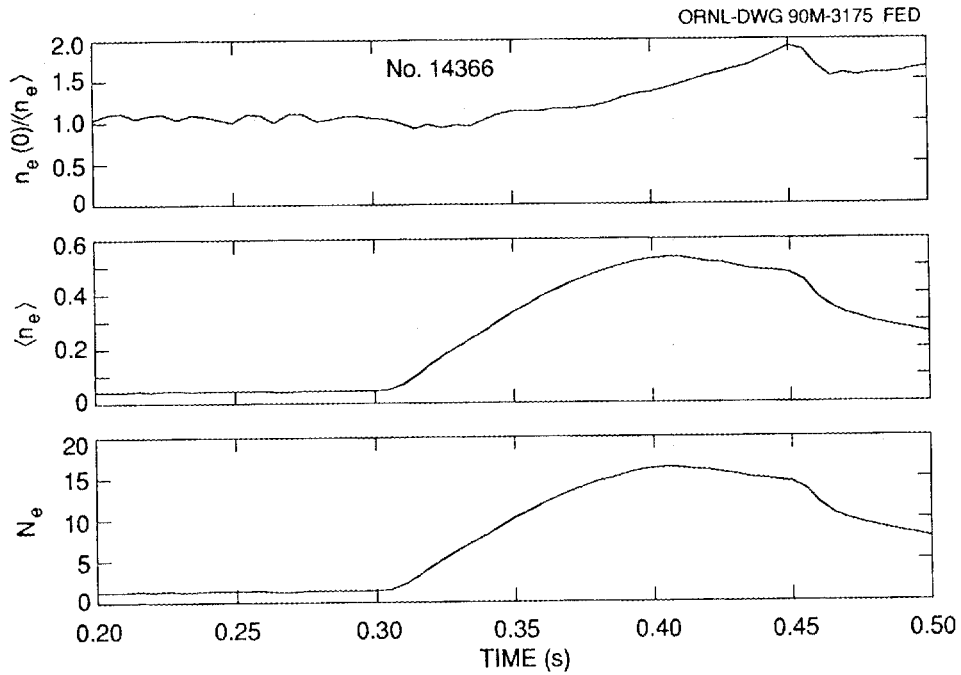


Fig. 4. The temporal evolution of the electron density peaking factor, volume-average density, and total number of electrons calculated from the inversion of the discharge in Fig. 3.

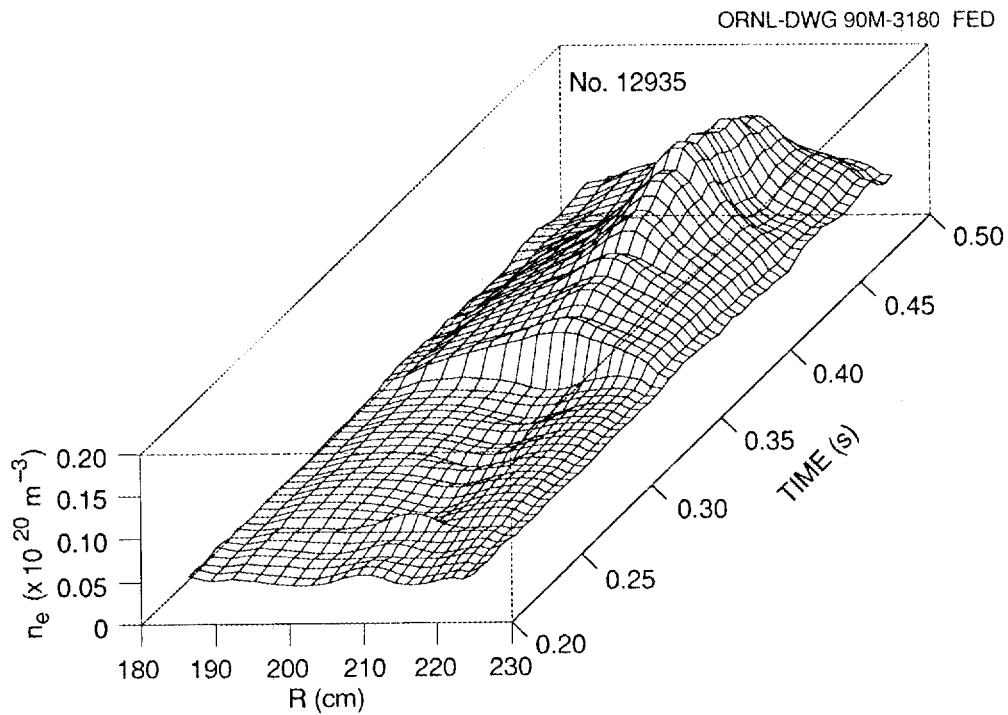


Fig. 5. The density profile evolution calculated by the inversion method for an ECH discharge with a pellet injected at 0.34 s.

pellet is injected at 0.33 s. The pellet causes the density profile to change from slightly hollow to peaked in the center; this peaked profile continues for the next 100 ms and in fact becomes more peaked owing to some as yet unexplained inward convection mechanism [10].

Density profiles obtained from the inversion method have been integrated along the path of a horizontal 2 mm interferometer on ATF that is shown in Fig. 6. This integrated line density compares favorably to the measured value as shown in Fig. 7 for the discharge shown in Fig. 5 with pellet injection. In general the calculated line integral of the density agrees to within 10% of the measured value, which is quite good considering the limited number of FIR interferometer channels currently available. The good agreement of the measured and calculated line integral densities gives us confidence in the inversion method and supports the hypothesis that the density is approximately constant on a flux surface.

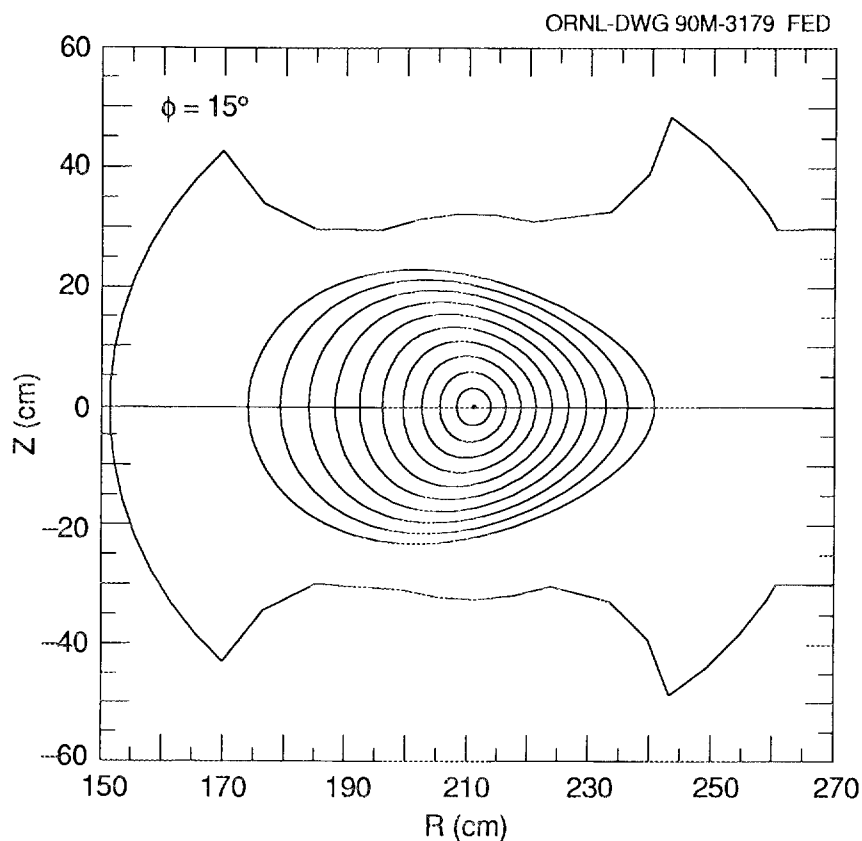


Fig. 6. The flux surface geometry halfway through a field period and path of the 2 mm interferometer on ATF. The toroidal angle $\phi = 15^\circ$.

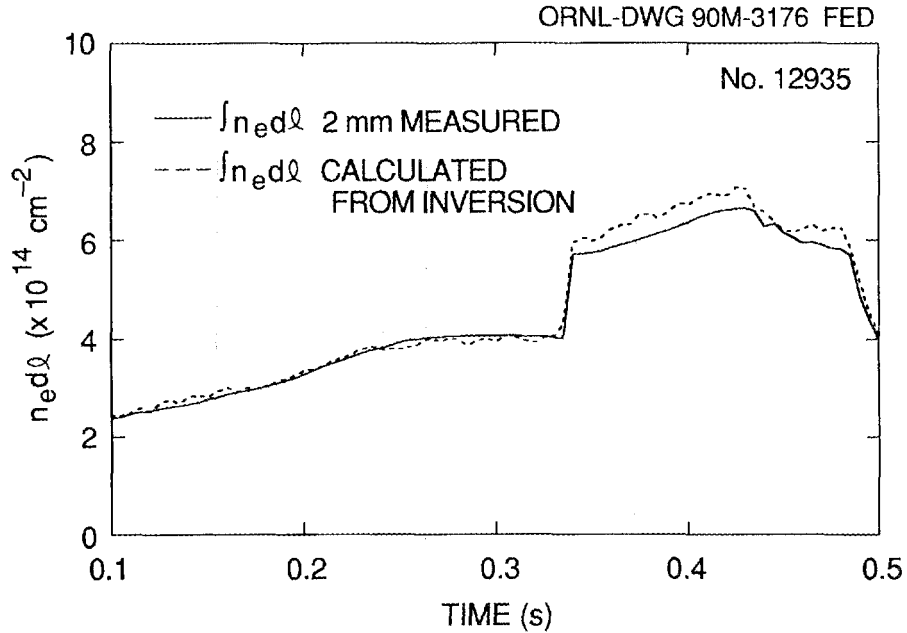


Fig. 7. Time dependence of the horizontal integration of the inverted density profile (dashed curve) and of the line integral density measured by the 2 mm interferometer during an ECH discharge with pellet injection at 0.34 s.

5.2 RADIATED POWER DENSITY PROFILES

The 15 channel bolometer array data are inverted in the same manner as described in Section 5.1 for the interferometer data. The primary difference is that the viewing chords of the bolometer are not vertical and therefore require calculation of the path length through both the top and bottom half of the flux surface geometry. Once the path length matrix is calculated from the TRACK subroutines, the inversion process is identical to that for the interferometer. As shown in Fig. 2, two of the chords do not generally intersect any of the closed flux surfaces of the ATF plasma and are not used in the inversion process.

An example of the bolometer array irradiance data is shown in Fig. 2 along with the finite-beta flux surface geometry. The resulting radiated power profile temporal evolution is shown in Fig. 8 for the entire discharge, which has two partial thermal collapses corresponding to drops in the measured plasma stored energy. It is common for the radiated power to become centrally peaked in

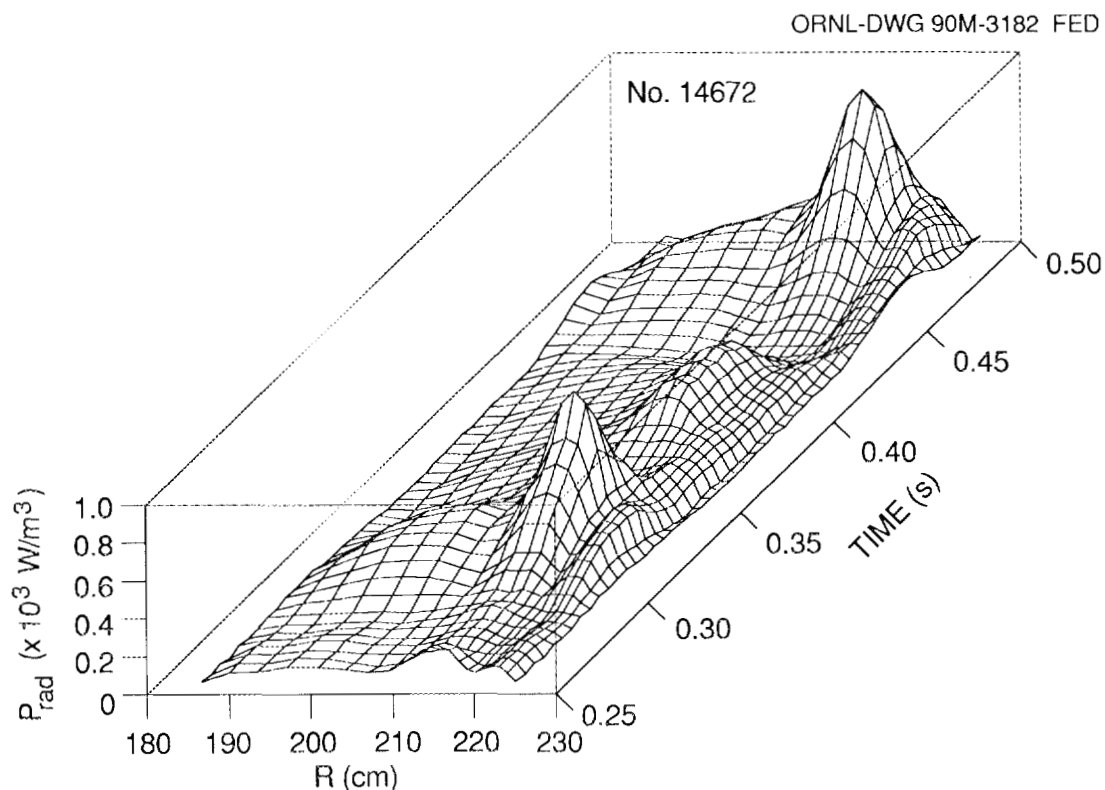


Fig. 8. The temporal evolution of the radiated power profile calculated from the inversion method for a discharge with thermal collapses at 300 and 450 ms.

ATF once a thermal collapse of the plasma has occurred. Analysis of a large number of discharges shows that there do not seem to be any strong in/out asymmetries in the radiated power density profiles. The inverted bolometer radiated power profiles have been compared with radiated power profiles derived from spectroscopic data [11] (impurity line radiation). The two profiles agree qualitatively in shape and within $\sim 15\%$ in magnitude of the total radiated power.

5.3 SENSITIVITY ANALYSIS

The sensitivity of this inversion method to variations in the flux surface geometry has been examined by inverting data with flux surfaces determined from different assumed plasma pressure profiles. By comparing the results of

these inversions, we find that the global shape of the inverted profile is not affected, but in/out asymmetry and the central profile shape can be sensitive to the choice of pressure profile. In general, errors due to small variations in the flux surface geometry used in the inversion process are not a significant factor. However, it is recommended that the experimentally determined finite-beta flux surface geometry be used for an accurate inversion.

A similar analysis of the sensitivity of the inversion method to measurement errors has been carried out. Both the interferometer and bolometer array data are subject to errors due to motion during the discharge, electronic noise, and other possible mechanisms. To test the sensitivity of the inversion process to these errors, we have performed the inversion on a set of measured bolometer array data as a reference. The data from one channel of the bolometer channels are then perturbed by adding 10% to and subtracting 10% from the measured value. The spline fit through the data is then recalculated and inverted. The results are then compared with the reference profile and are shown in Fig. 9 for a

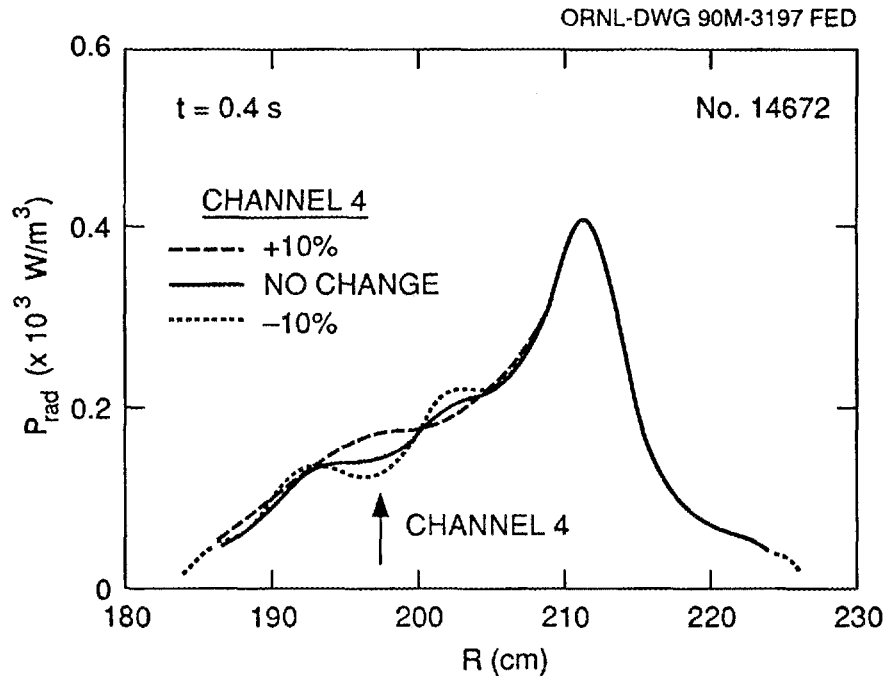


Fig. 9. Comparison of the inverted radiated power density profile (without perturbation) and profiles calculated with a perturbed irradiance at 197 cm. Note that there is a modest in/out asymmetry in the resulting radiated power density profile.

case with a peaked radiated power profile. We find that the propagation of such a perturbation, which is believed to be larger than the expected measurement errors, is well localized in the profile area where the perturbation is made, and its magnitude is on the order of that of the perturbation.

6. SUMMARY

The method developed by Park [4] for multichord interferometer inversion of tokamak data has been applied successfully to both FIR interferometer and bolometer array data from the ATF torsatron. It should be possible to apply the method in a similar fashion to other non-axisymmetric toroidal plasma confinement devices. The resulting profiles from the method are limited in resolution primarily by the number of chordal measurements available. The sensitivity of the method to the geometrical variations and measurement errors has been studied and is not found to be excessive for the types of errors expected.

The results of applying the method to ATF interferometer data show that density profiles during ECH-only portions of discharges are generally hollow, which is similar to results from other stellarator experiments. When NBI is applied, the density profiles are typically flat. Pellet injection has been used successfully to centrally peak the density profile in ECH discharges and has provided some peaking of the density profile during NBI. The results from bolometer array inversion indicate that the radiated power profiles in ATF are generally hollow but show strong central radiation after a thermal collapse of the plasma has occurred. The inverted radiated power profiles from the bolometer array data agree qualitatively with calculations of radiated power profiles from spectroscopic measurements of impurity radiation.

ACKNOWLEDGMENTS

We thank Drs. D. P. Hutchinson and K. L. Vander Sluis for help with the FIR interferometer, Dr. J. B. Wilgen for the 2 mm interferometer data, and Dr. S. Paul for the loan of the bolometer array used in this work. We appreciate the encouragement and useful suggestions of Drs. M. Murakami, H. Howe and W. A. Houlberg. We also thank the ATF operations and data acquisition groups for helping to provide the experimental data.

REFERENCES

- [1] LYON, J.F., CARRERAS, B.A., CHIPLEY, K.K., et al., Fusion Technol. **10** (1986) 179.
- [2] MA, C.H., HUTCHINSON, D.P., VANDER SLUIS, K.L., Rev. Sci. Instrum. **61** (10), Part II (1990) 2891.
- [3] PAUL, S.F., FONCK, R.J., SCHMIDT, G.L., Princeton Plasma Physics Lab. Rep. PPPL-2432 (1987).
- [4] PARK, H.K., Plasma Phys. Controlled Fusion **31** (1989) 2035.
- [5] GOLDFINGER, R.C., personal communication.
- [6] HIRSHMAN, S.P., VAN RIJ, W.I., MERKEL, P., Comput. Phys. Commun. **43** (1986) 143.
- [7] RASMUSSEN, D.A., ENGLAND, A.E., BAYLOR, L.R., et al., to be published.
- [8] ATTENBERGER, S.E., HOULBERG, W.A., HIRSHMAN, S.P., J. Comput. Phys., **72** (1987) 435.
- [9] COLCHIN, R.J., MURAKAMI, M., ANABITARTE, E., et al., Phys. Fluids B **2** (1990) 1347.
- [10] QUALLS, A.L., WILGEN, J.B., STEVENS, P.N., et al., Bull. Am. Phys. Soc. **35** (1990) 2060.
- [11] ISLER, R.C., personal communication.

INTERNAL DISTRIBUTION

1. Director, Fusion Energy Division
2. C. C. Baker
3. M. J. Saltmarsh
4. L. A. Berry
5. B. A. Carreras
6. R. A. Dory
7. J. L. Dunlap
8. H. H. Haselton
9. M. S. Lubell
10. T. E. Shannon
- 11-12. Laboratory Records Department
13. Laboratory Records, ORNL-RC
- 14-15. Central Research Library
16. Document Reference Section
17. Fusion Energy Division Library
- 18-19. ET/FE Division Publications Office
20. ORNL Patent Office
- 21-25. L. R. Baylor
- 26-27. C. H. Ma
- 28-29. S. Hiroe
30. S. E. Attenberger
31. R. C. Goldfinger
32. D. P. Hutchinson
33. R. C. Isler
34. K. L. Vander Sluis
35. J. B. Wilgen
36. M. Murakami
37. W. A. Houlberg
38. A. L. Qualls
39. D. A. Rasmussen
40. R. J. Wood

EXTERNAL DISTRIBUTION

41. S. Paul, Princeton Plasma Physics Laboratory, P.O. Box 451, Princeton, NJ 08543
42. Office of the Assistant Manager for Energy Research and Development, U.S. Department of Energy, Oak Ridge Operations Office, P.O. Box E, Oak Ridge, TN 37831
43. J. D. Callen, Department of Nuclear Engineering, University of Wisconsin, Madison, WI 53706-1687

44. R. W. Conn, Department of Chemical, Nuclear, and Thermal Engineering, University of California, Los Angeles, CA 90024
45. N. A. Davies, Acting Director, Office of Fusion Energy, Office of Energy Research, ER-50 Germantown, U.S. Department of Energy, Washington, DC 20545
46. S. O. Dean, Fusion Power Associates, Inc., 2 Professional Drive, Suite 248, Gaithersburg, MD 20879
47. H. K. Forsen, Bechtel Group, Inc., Research Engineering, P. O. Box 3965, San Francisco, CA 94119
48. J. R. Gilleland, L-644, Lawrence Livermore National Laboratory, P.O. Box 5511, Livermore, CA 94550
49. R. W. Gould, Department of Applied Physics, California Institute of Technology, Pasadena, CA 91125
50. R. A. Gross, Plasma Research Laboratory, Columbia University, New York, NY 10027
51. D. M. Meade, Princeton Plasma Physics Laboratory, P.O. Box 451, Princeton, NJ 08543
52. M. Roberts, International Programs, Office of Fusion Energy, Office of Energy Research, ER-52 Germantown, U.S. Department of Energy, Washington, DC 20545
53. W. M. Stacey, School of Nuclear Engineering and Health Physics, Georgia Institute of Technology, Atlanta, GA 30332
54. D. Steiner, Nuclear Engineering Department, NES Building, Tibbetts Avenue, Rensselaer Polytechnic Institute, Troy, NY 12181
55. R. Varma, Physical Research Laboratory, Navrangpura, Ahmedabad 380009, India
56. Bibliothek, Max-Planck Institut für Plasmaphysik, Boltzmannstrasse 2, D-8046 Garching, Federal Republic of Germany
57. Bibliothek, Institut für Plasmaphysik, KFA Jülich GmbH, Postfach 1913, D-5170 Jülich, Federal Republic of Germany
58. Bibliothek, KfK Karlsruhe GmbH, Postfach 3640, D-7500 Karlsruhe 1, Federal Republic of Germany
59. Bibliotheque, Centre de Recherches en Physique des Plasmas, Ecole Polytechnique Fédérale de Lausanne, 21 Avenue des Bains, CH-1007 Lausanne, Switzerland
60. J. Tachon, CEN/Cadarache, Departement de Recherches sur la Fusion Contrôlée, F-13108 Saint-Paul-lez-Durance Cedex, France
61. Bibliothèque, CEN/Cadarache, F-13108 Saint-Paul-lez-Durance CEDEX, France
62. Library, AEA Fusion, Culham Laboratory, Abingdon, Oxon OX14 3DB, England
63. Library, JET Joint Undertaking, Abingdon, Oxon OX14 3EA, England
64. Library, FOM-Instituut voor Plasmafysica, Rijnhuizen, Edisonbaan 14, 3439 MN Nieuwegein, The Netherlands
65. Library, National Institute for Fusion Science, Chikusa-ku, Nagoya 464-01, Japan

66. Library, International Centre for Theoretical Physics, P.O. Box 586, I-34100 Trieste, Italy
67. Library, Centro Richerche Energia Frascati, C.P. 65, I-00044 Frascati (Roma), Italy
68. Library, Plasma Physics Laboratory, Kyoto University, Gokasho, Uji, Kyoto 611, Japan
69. Plasma Research Laboratory, Australian National University, P.O. Box 4, Canberra, A.C.T. 2601, Australia
70. Library, Japan Atomic Energy Research Institute, Naka Fusion Research Establishment, 801-1 Mukoyama, Naka-machi, Naka-gun, Ibaraki-ken, Japan
71. G. A. Eliseev, I. V. Kurchatov Institute of Atomic Energy, P.O. Box 3402, 123182 Moscow, U.S.S.R.
72. V. A. Glukhikh, Scientific-Research Institute of Electro-Physical Apparatus, 188631 Leningrad, U.S.S.R.
73. I. Shpigel, Institute of General Physics, U.S.S.R. Academy of Sciences, Ulitsa Vavilova 38, Moscow, U.S.S.R.
74. D. D. Ryutov, Institute of Nuclear Physics, Siberian Branch of the Academy of Sciences of the U.S.S.R., Sovetskaya St. 5, 630090 Novosibirsk, U.S.S.R.
75. O. Pavlichenko, Kharkov Physical-Technical Institute, Academical St. 1, 310108 Kharkov, U.S.S.R.
76. Deputy Director, Southwestern Institute of Physics, P.O. Box 15, Leshan, Sichuan, China (PRC)
77. Director, The Institute of Plasma Physics, P.O. Box 26, Hefei, Anhui, China (PRC)
78. R. A. Blanken, Experimental Plasma Research Branch, Division of Applied Plasma Physics, Office of Fusion Energy, Office of Energy Research, ER-542, Germantown, U.S. Department of Energy, Washington, DC 20545
79. R. A. E. Bolton, IREQ Hydro-Quebec Research Institute, 1800 Montee Ste.-Julie, Varennes, P.Q. JOL 2P0, Canada
80. D. H. Crandall, Director, Division of Applied Plasma Physics, Office of Fusion Energy, Office of Energy Research, ER-542, Germantown, U.S. Department of Energy, Washington, DC 20545
81. R. L. Freeman, General Atomics, P.O. Box 85608, San Diego, CA 92138-5608
82. R. F. Gandy, Physics Department, Auburn University, Auburn, AL 36849
83. K. W. Gentle, RLM 11.222, Institute for Fusion Studies, University of Texas, Austin, TX 78712
84. R. J. Goldston, Princeton Plasma Physics Laboratory, P.O. Box 451, Princeton, NJ 08543
85. J. C. Hosea, Princeton Plasma Physics Laboratory, P.O. Box 451, Princeton, NJ 08543
86. D. Markevich, Division of Applied Plasma Physics, Office of Fusion Energy, Office of Energy Research, ER-55, Germantown, U.S. Department of Energy, Washington, DC 20545
87. R. H. McKnight, Experimental Plasma Research Branch, Division of Applied Plasma Physics, Office of Fusion Energy, Office of Energy Research, ER-542, Germantown, U.S. Department of Energy, Washington, DC 20545

88. E. Oktay, Division of Confinement Systems, Office of Fusion Energy, Office of Energy Research, ER-55, Germantown, U.S. Department of Energy, Washington, DC 20545
89. D. Overskei, General Atomics, P.O. Box 85608, San Diego, CA 92138-5608
90. R. R. Parker, Plasma Fusion Center, NW 16-288, Massachusetts Institute of Technology, Cambridge, MA 02139
91. W. L. Sadowski, Fusion Theory and Computer Services Branch, Division of Applied Plasma Physics, Office of Fusion Energy, Office of Energy Research, ER-541, Germantown, U.S. Department of Energy, Washington, DC 20545
92. J. W. Willis, Division of Confinement Systems, Office of Fusion Energy, Office of Energy Research, ER-55, Germantown, U.S. Department of Energy, Washington, DC 20545
93. A. P. Navarro, Division de Fusion, CIEMAT, Avenida Complutense 22, E-28040 Madrid, Spain
94. Laboratory for Plasma and Fusion Studies, Department of Nuclear Engineering, Seoul National University, Shinrim-dong, Gwanak-ku, Seoul 151, Korea
95. J. L. Johnson, Plasma Physics Laboratory, Princeton University, P.O. Box 451, Princeton, NJ 08543
96. L. M. Kovrizhnykh, Institute of General Physics, U.S.S.R. Academy of Sciences, Ulitsa Vavilova 38, 117924 Moscow, U.S.S.R.
97. O. Motojima, National Institute for Fusion Science, Chikusa-ku, Nagoya 464-01, Japan
98. S. Okamura, Institute of Plasma Physics, Nagoya University, Chikusa-ku, Nagoya 464, Japan
99. V. D. Shafranov, I. V. Kurchatov Institute of Atomic Energy, P.O. Box 3402, 123182 Moscow, U.S.S.R.
100. J. L. Shoet, Torsatron/Stellarator Laboratory, University of Wisconsin, Madison, WI 53706
101. H. Wobig, Max-Planck Institut für Plasmaphysik, D-8046 Garching, Federal Republic of Germany
- 102–154. Given distribution as shown in OSTI-4500, Magnetic Fusion Energy (Category Distribution UC-426, Experimental Plasma Physics)